Ferroelectric phase transition in RbH_2PO_4: Picosecond time-resolved impulsive stimulated Brillouin scattering experiments

Lap-Tak Cheng and Keith A. Nelson
Department of Chemistry, Massachusetts Institute of Technology, Cambridge, Massachusetts 02139
(Received 6 April 1987)

The anomalous acoustic behavior of rubidium dihydrogen phosphate near its ferroelectric phase transition was studied using "impulsive" stimulated Brillouin scattering with several scattering angles between 5.05° and 32.2°. The C_{66} shear elastic stiffness constant in the high-temperature phase showed elastic Curie-Weiss behavior, as expected on the basis of mean-field (MF) theory of the phase transition. Logarithmic corrections to MF behavior, suggested by other reports, were not observed to within 0.01 K of T_c. The p_{66} photoelastic constant also showed MF behavior. The polarization relaxation-time divergence was consistent with Landau-Khalatnikov theory, i.e., $\tau \sim (T-T_0)^{-1}$ over a substantial temperature range. Our observations are in agreement with those made on other KDP-family crystals, and with theoretical expectations for uniaxial ferroelectrics which are also ferroelastic in the low-temperature phase.

I. INTRODUCTION

Among the most extensively studied structural phase transitions are those in potassium dihydrogen phosphate (KH_2PO_4, abbreviated KDP) and its isomorphs. Despite detailed study of the complex soft-mode structure in these crystals, major open questions remain about the microscopic mechanism of the phase transitions.[1] However, almost all experimental and theoretical results obtained to date are in agreement about the validity of a mean-field (MF) description of the KDP-family transition.[2,3] This indicates suppression of critical fluctuations in the order parameter,[3] electric polarization (P_3), and in quantities coupled to it, as the transition temperature T_c is approached.

One member of the KDP family, rubidium dihydrogen phosphate (RDP), is of special interest because it has a truly second-order phase transition at ambient pressure. This makes RDP well suited for the study of critical behavior close to T_c. Logarithmic corrections to MF behavior in RDP have been reported based on specific-heat measurements in the ferroelectric phase[4] and more recently on dielectric constant measurements in the high-temperature, paraelectric phase.[5] These measurements appeared to support theoretical results on uniaxial ferroelectric phase transitions. In particular, the divergence of the order-parameter susceptibility (i.e., the dielectric constant ϵ_{33}) as $T \rightarrow T_c$ was predicted by Larkin and Khmel'nitskii (LK) to show logarithmic corrections for order-disorder transitions, yielding the temperature-dependent form[6]

$$\epsilon_{33}(T)=\frac{C}{T-T_c}\left[1+g\ln\frac{\Delta T}{T-T_c}\right]^{1/3}, \quad (1)$$

where C is the Curie constant above T_c, and g and ΔT are constants characteristic of the material. The theory is based on the fact that for uniaxial ferroelectrics, the depolarization field arising from long-range dipole-dipole interactions along the ferroelectric axis restricts fluctuations of the dipole moment along that axis only. The logarithmic correction to mean-field behavior results from this anisotropic suppression of critical fluctuations. The LK theory has subsequently been confirmed by renormalization-group calculations[7] which showed that for uniaxial ferroelectric phase transitions, the marginal dimensionality is equal to the spatial dimension, leading to mean-field behavior with logarithmic corrections.

However, as pointed out by its authors, the LK theory does not take into account coupling between the electric polarization and acoustic phonons, particularly those with wave vector lying along the basal plane. Renormalization-group calculations[8] subsequently showed that for uniaxial ferroelectrics that are also ferroelastics involving only one soft elastic constant, the marginal dimensionality of such a system is 2.5, less than the spatial dimension. Therefore mean-field theory should describe the phase transitions in such materials. Physically, the long-range interactions of the soft acoustic phonon strongly suppress critical fluctuations. The result is a lowering of the marginal dimensionality. In RDP, as in KDP and KD*P (KD_2PO_4), the polarization mode P_3 and the S_6 shear strain are bilinearly coupled through the a_{36} piezoelectric stress constant. The acoustic instability of S_6 should cause the transition to be mean field. Therefore, the observed logarithmic corrections to mean-field behavior are not anticipated by theory. In KDP and KD*P, dielectric and other measurements reported to date have consistently yielded mean-field results.[2]

We have undertaken a study of the S_6 acoustic-phonon behavior in RDP. An understanding of the RDP phase transition is important in its own right, as discussed above, and also in connection with the more complex mixed crystals, RDP-RD*P (Ref. 9) and RDP-ADP (Ref. 10), where $A=NH_4^+$. RDP represents an

important reference point for the mixed systems, whose "structural glass" properties have received considerable attention recently.[11]

Measurements of soft acoustic-phonon properties near structural phase transitions are often difficult for several reasons. First, ultrasonic measurements are often frustrated by the dramatic increase in acoustic attenuation $\gamma(T)$ as $T \rightarrow T_c$. Second, Brillouin-scattering measurements are made difficult by the softening of the acoustic frequency $\omega(T)$ and the increase in acoustic attenuation near T_c. These effects cause the Brillouin lines to broaden and move closer to the Rayleigh line (whose width and intensity are also highly temperature dependent) as $T \rightarrow T_c$. Often the Rayleigh and Brillouin features merge near T_c, and accurate determination of acoustic properties becomes difficult.[2]

Recently, an alternative time-domain light-scattering method has been developed and used to characterize soft acoustic-phonon behavior.[12,13] Through "impulsive" stimulated Brillouin scattering (ISBS), coherent acoustic phonons of selected polarization, wave vector, and orientation are excited optically with picosecond light pulses, and their time-dependent oscillations and decay are observed directly in the time domain. ISBS has been used for study of soft-mode behavior in KDP (Ref. 12) and KD*P (Ref. 13). The experiment can be carried out even in cases of extremely strong acoustic damping, and with a wide range of acoustic wave vectors which "connects" the frequency regimes usually probed by ultrasonics and Brillouin scattering.

In this paper we report ISBS results from RDP at temperatures between 300 K and $T_c \approx 147$ K. We find that the softening of $C_{66}(T)$ and the divergence of $p_{66}(T)$ can be explained in terms of mean-field theory. We also report on the critical slowing down of the polarization relaxation time at constant strain, $\tau(T)$, determined from acoustic attenuation measurements. We find that $\tau \sim \tau_0 (T - T_0)^{-1}$, where T_0 is the "clamped" transition temperature and $\tau_0 = 30$ ps. This result further supports a mean-field description of the phase transition.

II. THEORY

A. The ISBS experiment

The ISBS experiment is illustrated schematically in Fig. 1. Two picosecond laser pulses from the same laser, of central frequency and wave vectors $(\omega_1, \mathbf{k}_1)$ and $(\omega_1, \mathbf{k}_2)$, are overlapped spatially and temporally inside the sample to excite coherent acoustic phonons of frequency and (difference) wave vectors $(\omega_a, \pm \mathbf{q}_0)$, where $\mathbf{q}_0 = \mathbf{k}_1 - \mathbf{k}_2$ and $\omega_a / \mathbf{q}_0 = v_a(\mathbf{q}_0)$, the acoustic velocity. The excitation pulse duration t_L must be short compared to a single acoustic oscillation cycle for effective phonon generation to occur. In this case, the crossed pulses exert a spatially periodic, temporally impulsive force on the acoustic vibrational mode[14,15] through stimulated Brillouin scattering. The time-dependent material response is an acoustic standing wave described by

$$S(\mathbf{r},t) \propto \frac{p}{\omega_a} e^{-\gamma t} \sin(\omega_a t) \cos(\mathbf{q}_0 \cdot \mathbf{r}) \propto p G^s(\mathbf{r},t) \tag{2}$$

or

$$S(\mathbf{q},t) \propto \frac{p}{\omega_a} e^{-\gamma t} \sin(\omega_a t) [\delta(\mathbf{q} \pm \mathbf{q}_0)] \propto p G^s(\mathbf{q},t) , \tag{3}$$

where S is acoustic strain, p is the appropriate photoelastic constant, and G^s is the impulse response function for an underdamped acoustic mode. Equation (2) or (3) describes a standing-wave oscillation of frequency and wave vectors $(\omega_a, \pm \mathbf{q}_0)$. The strain amplitude depends linearly on the photoelastic constant p which couples the optical and acoustic fields, and inversely on ω_a.

The acoustic standing-wave displacements modulate the dielectric constant ϵ whose response $\delta\epsilon(\mathbf{q},t)$ can be described by the response function $G^{\epsilon\epsilon}(\mathbf{q},t) \sim \delta\epsilon(\mathbf{q},t) \sim pS(\mathbf{q},t)$. This modulation gives rise to a time-dependent volume "grating" which can coherently scatter or "diffract" a variably delayed probe pulse incident at the phase-matching geometry. The intensity of diffracted probe light is measured in the ISBS experiment, yielding a time-dependent signal of the form[15,16]

$$I(\mathbf{q},t) \propto | G^{\epsilon\epsilon}(\mathbf{q},t) |^2 . \tag{4}$$

For a single acoustic mode, $G^{\epsilon\epsilon}(\mathbf{q},t) \propto p G^s(\mathbf{q},t)$, and

$$I(\mathbf{q},t) \propto p^4 [G^s(\mathbf{q},t)]^2 \propto \frac{p^4}{\omega_a^2} [e^{-\gamma t} \sin(\omega_a t)]^2 . \tag{5}$$

From Eq. (5) it is apparent that the time-dependent ISBS signal $I(\mathbf{q},t)$ from underdamped acoustic phonons shows time-dependent oscillations at twice the standing-wave frequency ω_a, and decays at twice the acoustic attenua-

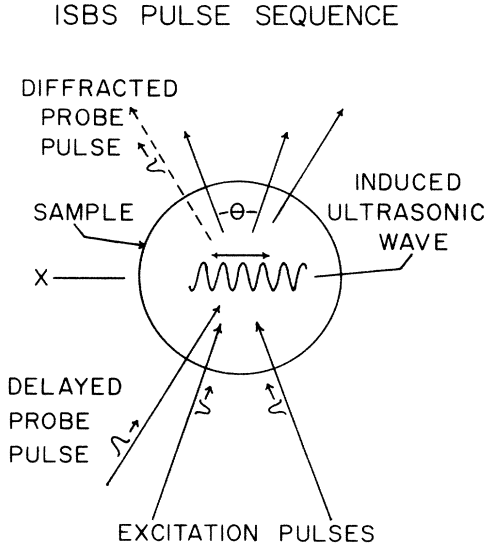

FIG. 1. Schematic diagram of the ISBS experiment. The crossed excitation pulses "impulsively" excite an ultrasonic standing wave in the sample. The standing-wave oscillations and decay are monitored by diffraction of variably delayed probe pulses.

tion rate γ. The signal intensity is proportional to the fourth power of the photoelastic constant and inversely proportional to ω_a^2.

In general, ISBS excitation with scattering wave vector $\mathbf{q}_0$ could result in excitation of any or all of the three acoustic modes with that wave vector. However, along pure acoustic-mode directions, mode-selective excitation is possible through experimental control of the excitation-pulse polarizations.[13] In all of the RDP experiments discussed below, the scattering wave vector was aligned along one of the equivalent a axes of the tetragonal crystal, and the scattering plane was coincident with the crystallographic ac plane. In this configuration, two vertically polarized (V-V) excitation pulses would excite the pure C_{11} longitudinal wave, while the vertically and horizontally (V-H) polarized excitation pulses actually used excited the pure C_{66} transverse acoustic mode.[12,13] The appropriate strain, photoelastic, and dielectric constant components are S_6, p_{66}, and ϵ_{12}, respectively. The ϵ_{12} "grating" rotated the polarization of the H-polarized probe pulse to yield V-polarized diffracted signal. The ISBS experiment is in this case a time-domain, stimulated analog of frequency-domain, spontaneous V-H Brillouin scattering from thermally excited transverse phonons. A detailed comparison between impulsive stimulated scattering (ISS) and conventional light scattering has been carried out.[15,16]

B. Coupled modes in RDP and in ISS experiments

Equation (4) is a general result which applies to impulsive stimulated scattering signal from any type of material mode. ISS data from optic phonons,[17] molecular vibrations,[18] and orientational modes[19] have been collected.[15] In general, more than one mode may be coherently excited and probed in an ISS experiment. For coupled-mode systems such as RDP, the dielectric response is given by

$$G^{\epsilon\epsilon}(\mathbf{q},t)=\sum_{\alpha,\beta} a^{\alpha}a^{\beta}G^{\alpha\beta}(\mathbf{q},t) , \tag{6}$$

where a^{α} and a^{β} are differential polarizabilities and $G^{\alpha\beta}$ are coupled-mode response functions. In general, the full form of the dielectric response must be used when analyzing ISS data.

The equations of motion for the bilinearly coupled polarization mode and shear acoustic mode driven by an optical field are

$$\rho\ddot{u}-C_{66}^{P}\frac{\partial^2 u}{\partial r^2}+a_{36}\frac{\partial P_3}{\partial r}=\frac{1}{8\pi}p_{66}\frac{\partial}{\partial r}\mathbf{DD} , \tag{7}$$

$$\dot{P}_3-\frac{1}{\tau}P_3-\frac{a_{36}\epsilon^{33}}{\tau}\frac{\partial u}{\partial r}=-\frac{1}{8\pi}\frac{r_{63}\epsilon^{33}}{\tau}\mathbf{DD} , \tag{8}$$

where u is the acoustic displacement, ρ is the mass density, C_{66}^{P} is the high temperature (constant polarization) elastic stiffness constant, r_{63} is the electro-optic stress coefficient, and $\mathbf{D}$ is the electric displacement. The relaxation time τ and dielectric susceptibility ϵ_{33} for the uncoupled (constant strain or "clamped") polarization mode are the only temperature-dependent quantities. Acoustic attenuation in the absence of coupling has been neglected in Eq. (7). The polarization mode, which in KDP-family crystals is heavily overdamped near T_c, has been described approximately in Eq. (8) in terms of a relaxation time $\tau(T)$. The impulse response can be expressed in terms of the four coupled-mode response functions $G^{\alpha\beta}(\mathbf{q},t)$ (where α and β are S or P), given by

$$G^{\alpha\beta}(\mathbf{q},t>0)=[A^{\alpha\beta}e^{-\gamma t}+B^{\alpha\beta}e^{-\gamma t}\sin(\omega_a t)]\delta(\mathbf{q}\pm\mathbf{q}_0) , \tag{9}$$

assuming that the vibrational part of the response remains underdamped. Solution for the amplitudes, $A^{\alpha\beta}$ and $B^{\alpha\beta}$, and the dynamical parameters, λ, ω_a, and γ, is lengthy but straightforward. In the limit $\omega_a\tau\ll 1$, relevant to the experiments discussed below, the standard expressions for ω_a and γ are reached:

$$\omega_a^2+\gamma^2=\frac{q^2}{\rho}(C_{66}^{P}-\epsilon_{33}a_{36}^2)\equiv\frac{q^2}{\rho}C_{66}^{E} , \tag{10}$$

$$\gamma=\frac{\epsilon_{33}a_{36}^2q^2\tau}{2\rho} , \tag{11}$$

where $C_{66}^{E}(T)$ is the elastic constant at constant field. In our experiments, the excitation and probe laser pulse durations were always long compared to the relaxational part of the coupled-mode response, i.e., $\tau_L>\lambda^{-1}\approx\tau$, so this part of the response could not be time resolved. The pulse durations were short compared to the vibrational response, i.e., $\tau_L<2\pi/\omega_L$, so the time-dependent signal assumed the simple form shown in Eq. (5). Equations (10) and (11) were used to extract $C_{66}^{E}(T)$, $\epsilon_{33}(T)$, and $\tau(T)$ from the measured values of $\omega_a(T)$ and $\gamma_a(T)$. The signal intensity was measured to yield $p_{66}^{E}(T)$, which is related to $\epsilon_{33}(T)$ according to[12]

$$p_{66}^{E}(T)=p_{66}^{P}+r_{36}a_{36}\epsilon_{33}(T) . \tag{12}$$

III. EXPERIMENTAL METHODS

The ISBS experimental setup is illustrated schematically in Fig. 2. A cw Nd:YAG laser (YAG denotes yttrium aluminum garnet) is acousto-optically mode-locked and Q-switched (at a 500-Hz repetition rate) to produce pulsetrains of 1.06-μm, 85-ps pulses with up to 80 μJ of energy. Three of the pulses are isolated from the pulsetrains by electro-optic Pockels cells. Two of the pulses are overlapped spatially and temporally inside the sample for ISBS excitation. The third pulse is frequency-doubled, variably delayed along a dc-motorized delay line, and used to probe the excitation region at the phase-matching angle. The diffracted signal is monitored by a photodiode and a lock-in amplifier whose output is stored by a personal computer. The optical delay line is double passed to provide a maximum delay of about 20 ns. To probe with longer delays, later pulses from the pulsetrain are selected. In this manner, delays of more than 200 ns are achieved.

The focusing of excitation and probe pulses into the

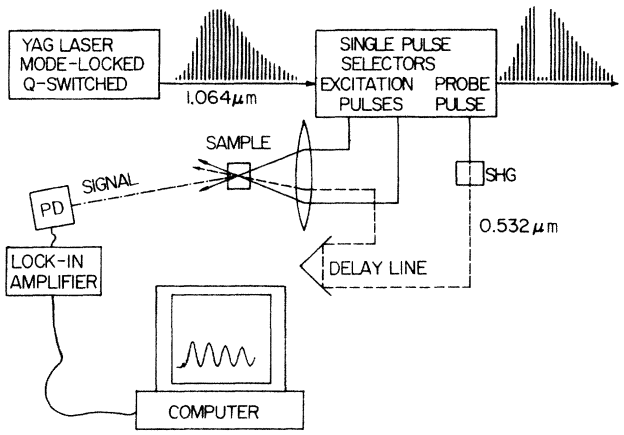

FIG. 2. ISBS experimental setup. See text for details. SHG, second-harmonic generator; PD, photodiode.

crystal was arranged with considerable care to minimize the range of acoustic wave vectors sampled in each experiment. In ISBS, focusing of the excitation pulses produces an acoustic "wave packet" whose spatial extent is limited by the spot sizes. The acoustic "standing wave" generated is actually composed of two counterpropagating, traveling waves which eventually propagate away from each other. This reduces the intensity of diffracted signal and alters its time dependence. Although the effects on signal can be calculated accurately,[16] measurement of low acoustic attenuation rates is difficult. In most RDP experiments, these effects were minimized by using cylindrically focused excitation pulses. The excitation region was an ellipse whose long axis (about 2 mm long) was aligned along $\mathbf{q}_0$. The short axis was focused to 200 μm to increase signal intensity. The probe pulse was focused to a round spot of 150-μm diameter. Attenuation rates as weak as about 50 dB/cm were measured accurately in this manner. Near T_c, the intrinsic damping was so strong that propagation effects were negligible. Round, 150-μm excitation spot sizes were used near T_c to minimize the effects of temperature variation and static inhomogeneities within the excitation volume. Some heating of the sample occurred through weak vibrational overtone absorption of the 1.06-μm excitation pulses. The extent of steady-state heating was estimated (by measuring intensity-dependent changes in ω_a) to be about 8 mK.

The RDP crystal is a $1\times1\times1$-cm^3 cube grown, cut, and with c faces polished by Cleveland Crystals. It is immersed in 2-methylbutane for index matching inside an aluminum cell with glass windows. The sample cell is surrounded by a radiation shield, and is cooled in a closed-cycle refrigerator. The temperature is monitored with calibrated Si diodes and is regulated by a Lakeshore controller. Short-term control of ±2 mK and long-term control of ±4 mK were achieved. The crystal was oriented such that $\mathbf{q}_0 \| a$ ($\pm0.5°$) by finding the "softest" acoustic mode near T_c. Experiments were carried out with scattering angles of 5.05°, 11.5°, 19.5°, 31.7°, and 32.2°. Note that "scattering angle" is defined here as the angle between the excitation pulses. The corresponding wave-vector magnitudes were 5.20×10^3, 1.18×10^4, 2.00×10^4, 3.23×10^4, and 3.27×10^4 cm^{-1}.

The entire experiment, including laser pulse selection, delay-line operation, data acquisition, and temperature regulation, is under computer control. Some of the data were collected overnight, with no operator present, while the computer varied the sample temperature and waited for it to stabilize, ran the experiment, and repeated the procedure. Typical data collection times ranged from as little as 30 s at temperatures near T_c, where strong signal permitted rapid delay-line scanning and strong acoustic damping called for only one pass of the delay line, to as much as 15 min when many slower scans of the delay line were necessary.

Data analysis was carried out by simulation with a damped harmonic-oscillator functional form as indicated by Eq. (5). Curve-fitting routines have been developed which account for finite laser pulse durations and the effects of finite laser spot sizes. However, the simple form in Eq. (5) yielded excellent fits to most of the data recorded.

IV. RESULTS AND DISCUSSION

ISBS data from RDP are shown in Figs. 3 and 4. The solid curves show experimental data, while the dashed curves (in Fig. 3 only) show computer simulations. Three sweeps are shown in Fig. 3, all taken under identical experimental conditions except for the sample temperature. For these temperatures near T_c, the excitation pulses were focused to round spots. The scattering angle was 31.7°. As expected, the acoustic frequency softens and the attenuation and signal intensity increase as $T\rightarrow T_c$. In most cases, such as Figs. 3(a) and 3(b), the data could be fit almost perfectly by a damped sinusoidal curve. The data shown in Fig. 3(c), recorded with the sample temperature at T_c+16 mK, showed deviations from damped harmonic oscillation. At temperatures this close to T_c, even small thermal fluctuations or inhomogeneities have noticeable effects on the data.

Figure 4 shows ISBS data taken at a higher temperature, with cylindrically focused excitation pulses and a 32.2° scattering angle. These data also yield an excellent fit to a damped sinusoidal curve. Some "beating" is apparent in the data due to weak excitation of the longitudinal acoustic mode.[15–17] Analysis of the data is still straightforward.

Figure 5 shows a plot of C_{66}^E versus T for the various scattering angles. C_{66}^E was calculated from the experimentally determined parameters, ω_a and γ, using expression (10) and a reported value of the density, $\rho=2.866$ g/cm^3.[20] The solid curve in Fig. 5 is a fit of the data using the mean-field expression,

$$C_{66}^E(T)=C_{66}^P\frac{T-T_c}{T-T_0} \tag{13}$$

with adjustable parameters C_{66}^P and T_0. The parameters yielding the best fit were $C_{66}^P=4.2\times10^{10}$ dyn/cm^2 and

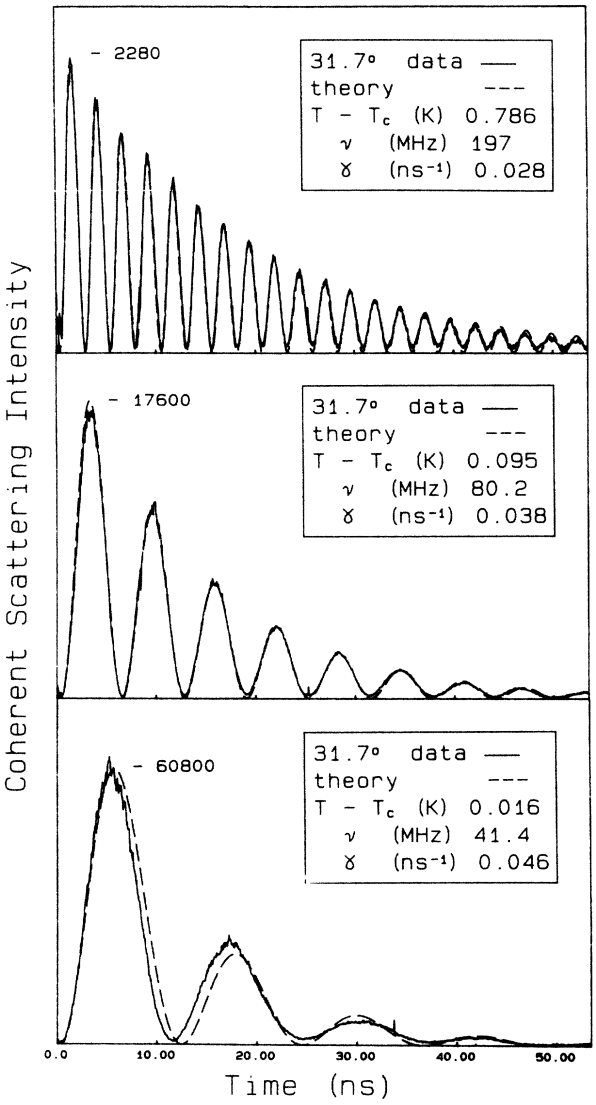

FIG. 3. ISBS data from the soft acoustic mode in RDP, taken with a 31.7° scattering angle. The solid curves show data taken at several temperatures within 1K of T_c. The dashed curves show computer-generated simulations of the data assuming $I(t)\sim[e^{-\gamma t}\sin(\omega_a t)]^2$ as indicated by Eq. (5), and where $\nu=\omega_a/2\pi$. As $T\rightarrow T_c$, the acoustic frequency softens, the attenuation rate increases, and the intensity of ISBS signal increases to more than 60 000 times its room-temperature value. The simulations fit the data extremely well in the first two sweeps and reasonably well in the third, which was taken at $T-T_c=16$ mK. Small temperature fluctuations and crystal inhomogeneities can influence the data at temperatures this close to T_c.

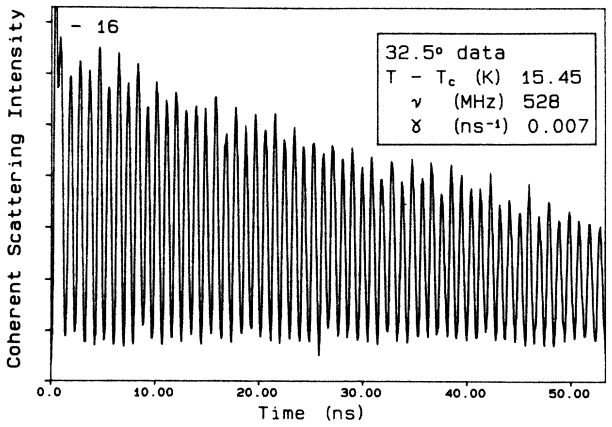

FIG. 4. ISBS data from the soft transverse-acoustic mode in RDP, taken with a 32.2° scattering angle and with cylindrical focusing of the excitation pulses. Despite some "beating" of transverse- and longitudinal-acoustic frequencies, the overall fit to a damped oscillator curve is still very good. The minima in signal intensity are nonzero due to the finite probe pulse duration.

$T_0=T_c-6.6$ K. Figure 6 shows a plot of $(C_{66}^P-C_{66}^E)^{-1}$ against temperature for the 32.2° data, and provides a direct comparison with dielectric measurements reported recently (Fig. 1 in Ref. 5). It is clear that the data can be fit quite well by mean-field theory. Logarithmic corrections would result in a bending of the data near T_c, which is not observed (see Fig. 6 inset). Data from other scattering angles also yielded linear plots with a range of slopes giving an uncertainty of ± 0.2 K for T_c-T_0. We believe the uncertainty is a result of slight misalignments of $\mathbf{q}_0$. Note that the magnitude of T_c-T_0 directly reflects the coupling strength of P_3 and S_6, i.e.,

$$T_c-T_0=\frac{a_{36}^2 C}{C_{66}^P}\ , \tag{14}$$

where C is the Curie constant. Using our results for C_{66}^P and T_0 and the reported value of $C=3800$ K,[21] we calculated $a_{36}=3.0\times10^4$ esu (cgs), comparable to the value in KDP.[22]

Our value of T_c-T_0 is considerably larger than some other reported values, which vary from 0.2 to 6.2 K. Dielectric measurements at 100 KHz (Ref. 23) and 10 KHz (Ref. 5) yielded values of 0.2 and 4 K, respectively. Brillouin-scattering results obtained at temperatures above T_c+2 K with a 90° scattering angle[24] yielded $T_c-T_0=1.6$ K. These results were apparently influenced by dynamic effects ($\omega_a\tau\approx1$) which reduced the softening of C_{66} and the divergence of p_{66} as $T\rightarrow T_c$. Finally, piezoelectric measurements[21] yielded $T_c-T_0=6.2$ K, in better agreement with our result.

Our results are based on careful measurements within 1 K of T_c, as well as many measurements at higher temperatures. Results obtained with several scattering angles showed no acoustic dispersion, indicating that our values of $C_{66}^E(T)$ are not influenced by dynamic effects which are important at higher acoustic frequencies. We note that uncertainty in the value of C_{66}^P will not significantly alter the linearity of the data in Fig. 6. Our data cannot be reconciled with the smaller values of T_c-T_0 previously reported.

Our extrapolated value of C_{66}^P actually exceeds by about 10% the room-temperature value, 3.8×10^{10}

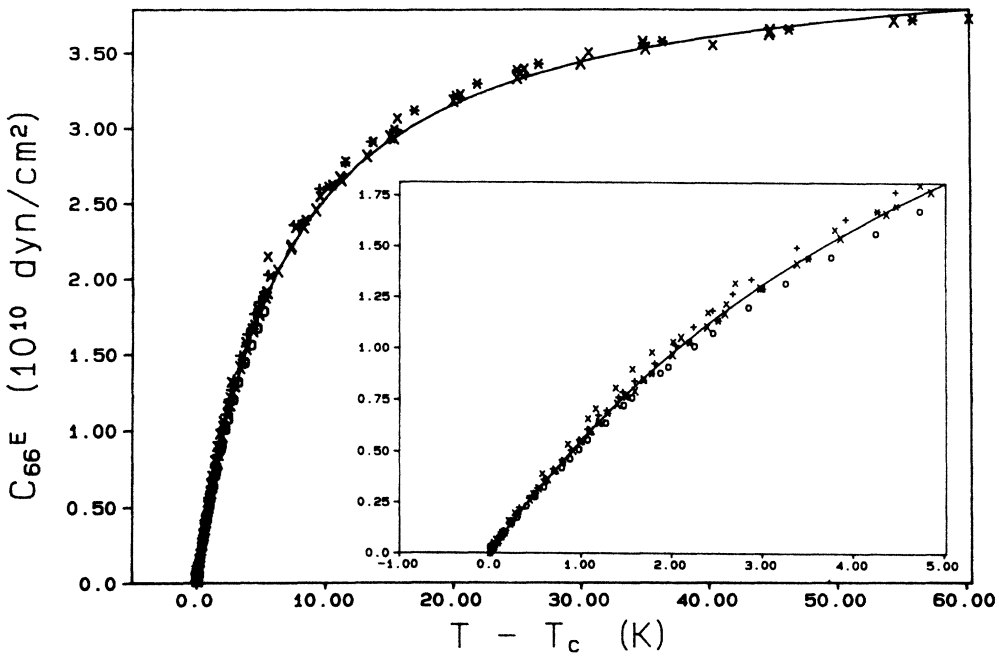

FIG. 5. C_{66}^{E} elastic constant vs T, determined by ISBS measurements at several scattering angles. The solid curve is a Curie-Weiss fit to the results using Eq. (13) with the parameters given in the text. The inset shows C_{66}^{E} vs $T-T_c$ on an expanded scale. x, 5.05° results; +, 11.5° results; *, 19.5° results; ○, 31.7° results; X, 32.2° results. All the results lie quite close to the solid curve. Small systematic variations in the results (for example, the 31.7° results showed slightly lower values) are due to small amounts of misalignment in the scattering wave vector. There is no significant acoustic dispersion in the wave-vector range covered.

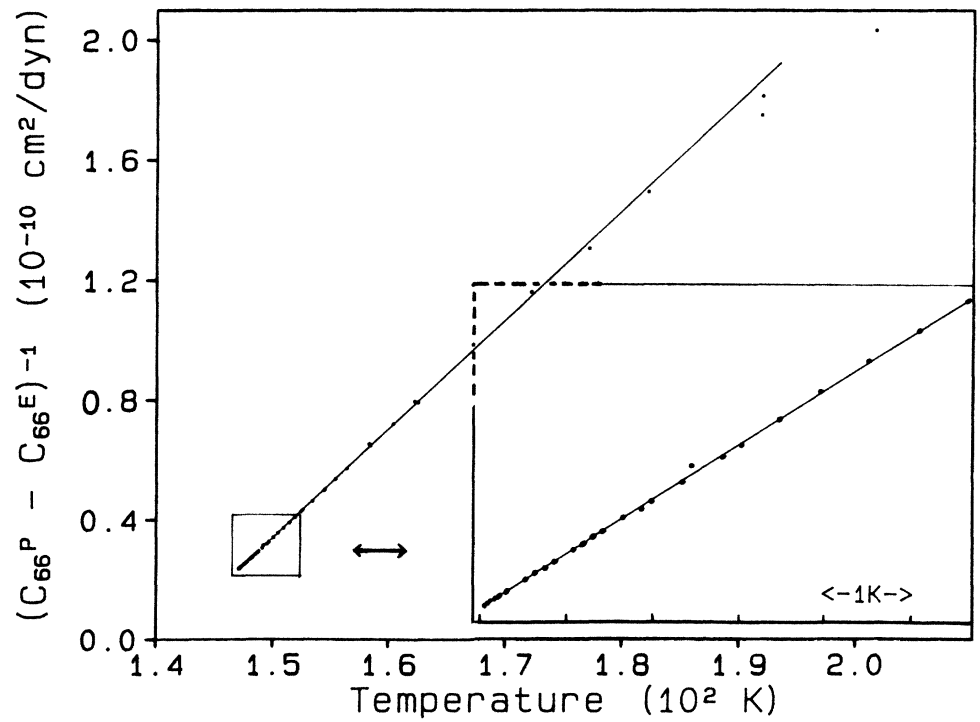

FIG. 6. $(C_{66}^{P}-C_{66}^{E}]^{-1}$ vs T, determined from data collected with a 32.2° scattering angle. The solid line is a guide to illustrate the linear T dependence.

dyn/cm^2, measured by us and others.[23,24] It seems likely that at high temperatures there is slight deviation in $\epsilon_{33}(T)$ from Curie-Weiss behavior, as has been noted earlier.[23]

Figure 7 shows relative values of the photoelastic constant p_{66}^E, calculated using Eq. (5) and data collected with the 32.2° scattering angle. Through Eq. (11), the behavior of $p_{66}^E(T)$ provides an independent determination of $\epsilon_{33}(T)$. Curie-Weiss theory again predicts linear variation of p_{66}^E versus $(T-T_0)^{-1}$. Although the data are somewhat scattered, linear behavior is still apparent in Fig. 7, and is consistent with the value $T_c-T_0=6.6$ K. In particular, no obvious bending of the data occurs near T_c.

Figure 8 shows values of the relaxation time calculated from Eq. (11), using data obtained with a 32.2° scattering angle. The measurement of weak acoustic attenuation remains the most demanding task in the ISBS experiment. Other than the finite spot sizes problem mentioned earlier, delay-line walk-off and probe spot size variation along the delay line add to the difficulty of measuring weak attenuation. Measurements were most accurate at large scattering angles and near T_c, where attenuation was strongest. Within experimental uncertainty, the data are consistent over a wide temperature range with Landau-Khalatnikov theory predicting $\tau=\tau_0/(T-T_0)$, with τ_0 determined to be 3×10^{-11} s K, comparable to that of KDP.[25] A sharp increase in attenuation is observed within 0.02 K of T_c with every scattering angle. The full solution of the coupled-mode equations (7) and (8) shows that this cannot be the result of dynamic effects which would occur if $\omega_a\tau\ll1$ no longer obtained. However, the increase could be caused by the $\sim$10-mK laser heating mentioned earlier, or by small crystal inhomogeneities. Near T_c, the temperature gradient across the excitation volume introduces a range of acoustic frequencies whose rapid dephasing causes a rapid decay of signal intensity. This effect, analogous to inhomogeneous broadening (due to laser heating or preexisting sample inhomogeneities) in frequency-domain

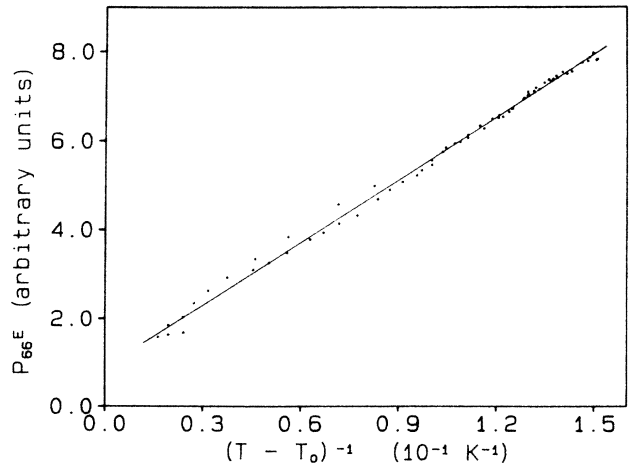

FIG. 7. Relative values of P_{66}^E vs $(T-T_0)^{-1}$, determined at 32.2° scattering angle. The solid line is a guide to illustrate the linear T dependence.

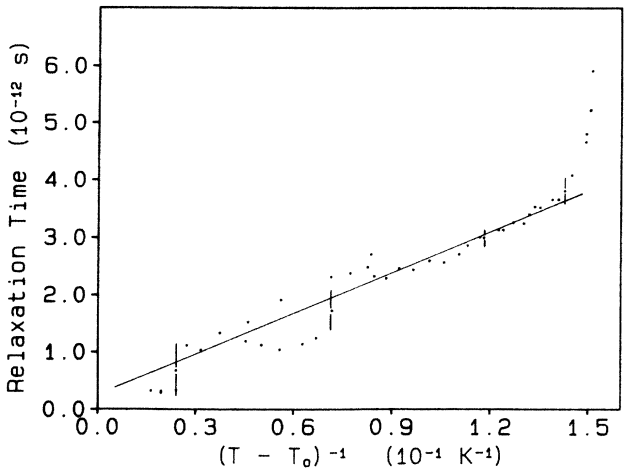

FIG. 8. Relaxation time τ vs $(T-T_0)^{-1}$, determined from data collected with a 32.2° scattering angle. The solid line is a fit of the data to the functional form $\tau=\tau_0/(T-T_0)$, yielding $\tau_0=3\times10^{-11}$ s K.

light scattering, adds to (and distorts) the decay due to intrinsic attenuation. Inhomogeneous dephasing can also cause a nonzero "baseline" in signal near T_c, as seen in Fig. 3(c). Because we cannot now separate inhomogeneous and homogeneous dephasing contributions near T_c, we do not consider it prudent to draw conclusions about $\tau(T)$ based on the observation of apparent anomalies in $\gamma(T)$. Experiments are underway to investigate this temperature region more carefully using 532-nm excitation pulses, which do not heat the sample significantly. Steps have also been taken to improve our accuracy in measuring weak attenuation.

We note that relative determination of T_c during each experiment was straightforward and reproducible to within our temperature stability limits of ±2 mK. Several changes were immediately apparent when the crystal entered the low-T phase. First, domain formation led to substantial elastic scattering of light by the crystal. This generally prevented further collection of data. However, data could occasionally be collected within a few mK below T_c. These data showed a sudden increase in the acoustic frequency, a decrease in the attenuation rate and signal intensity, and a "beating" pattern characteristic of ISBS data from two coherent acoustic modes. The last feature probably occurs because in the low-T, orthorhombic phase, $\mathbf{q}_0$ is no longer aligned along a crystallographic axis but is 45° between two inequivalent axes. The data recorded above T_c never showed history-dependent effects or any effects of the crystal having been in the low-T phase.

V. CONCLUSIONS

We have characterized the soft C_{66} acoustic mode of RDP at temperatures above T_c and found that elastic Curie-Weiss behavior obtains. The results of ISBS experiments with several scattering angles are in excellent agreement and indicate the validity of a mean-field

description of the RDP phase transition to within 10 mK of T_c. The temperature dependence of the p_{66} photoelastic constant was also determined, and the results further confirm mean-field behavior. Finally, the critical slowing down of the polarization relaxation time was found to follow Landau-Khalatnikov theory at temperatures above $T_c + 20$ mK. Deviations from this behavior may occur within 20 mK of T_c, but the present results in this range are inconclusive.

The mean-field critical behavior in RDP is similar to that found in other KDP-family crystals, and is in agreement with theoretical expectations for uniaxial ferroelectrics with soft acoustic modes.

ACKNOWLEDGMENTS

We thank B. Kohler for generous assistance in the development of computerized data analysis routines. This work was supported in part by grants from the National Science Foundation (No. DMR-8306701), Research Corporation, the Petroleum Research Fund, and TRW. K.A.N. acknowledges support from the A. P. Sloan Foundation.

[1]M. Tokunaga, Progr. Theor. Phys. (Suppl.) **80**, 156 (1984); M. Tokunaga and I. Tatsuzaki, Phase Transitions **4**, 97 (1984).

[2]KDP-family transitions are discussed extensively in M. E. Lines and A. M. Glass, *Principles and Applications of Ferroelectrics and Related Materials* (Clarendon, Oxford, 1977); and *Light Scattering Near Phase Transitions,* edited by H. Z. Cummins and A. P. Levanyuk (North-Holland, Amsterdam, 1983).

[3]A. D. Bruce and R. A. Cowley, *Structural Phase Transitions* (Taylor and Francis, London, 1981).

[4]M. A. Amin and B. A. Strukov, Fiz. Tverd. Tela (Leningrad) **10**, 3158 (1969) [Sov. Phys.—Solid State **10**, 2498 (1969)].

[5]J. L. Martinez and J. A. Gonzalo, Phys. Rev. B **32**, 400 (1985).

[6]A. I. Larkin and D. E. Khmelnitskii, Zh. Eksp. Teor. Fiz. **56**, 2087 (1969) [Sov. Phys.—JETP **29**, 1123 (1969)].

[7]A. Aharony, Phys. Rev. B **8**, 3363 (1973).

[8]R. A. Cowley, Phys. Rev. B **13**, 4877 (1976); R. Folk, H. Iro, and F. Schwabl, Z. Phys. B **25**, 69 (1976).

[9]J. L. Martinez, J. M. Calleja, and J. A. Gonzalo, Solid State Commun. **52**, 499 (1984).

[10]E. Courtens, Jpn. J. Appl. Phys. (Suppl. 24-2) **24**, 70 (1985).

[11]N. O. Birge, Y. H. Jeong, S. R. Nagel, S. Battacharya, and S. Susman, Phys. Rev. B **30**, 2306 (1984); S. D. Russell and R. Merlin, *ibid.* **33**, 1871 (1986).

[12]M. M. Robinson, Y.-X. Yan, E. B. Gamble, Jr., L. R. Williams, J. S. Meth, and K. A. Nelson, Chem. Phys. Lett. **112**, 491 (1984).

[13]M. R. Farrar, L.-T. Cheng, Y.-X. Yan, and K. A. Nelson, IEEE J. Quant. Electron. **QE - 22**, 1453 (1986).

[14]K. A. Nelson, J. Appl, Phys. **53**, 6060 (1982).

[15]Y.-X. Yan, L.-T. Cheng, and K. A. Nelson, in *Advances in Nonlinear Spectroscopy,* edited by R. J. H. Clark and R. E. Hester (Wiley, New York, 1987), p. 299.

[16]Y.-X. Yan and K. A. Nelson, J. Chem. Phys. **87**, 6240 (1987); **87**, 6257 (1987).

[17]S. DeSilvestri, J. G. Fujimoto, E. P. Ippen, E. B. Gamble, Jr., L. R. Williams, and K. A. Nelson, Chem. Phys. Lett. **116**, 146 (1985).

[18]S. Ruhman, A. G. Joly, and K. A. Nelson, J. Chem. Phys. **86**, 6563 (1987).

[19]L. R. Williams, S. Ruhman, A. G. Joly, B. Kohler, and K. A. Nelson, in *Advances in Laser Science II,* Proceedings of the 1986 International Laser Science Conference (AIP, New York, 1987), p. 408; S. Ruhman, L. R. Williams, A. G. Joly, B. Kohler, and K. A. Nelson, J. Phys. Chem. **91**, 2237 (1987).

[20]G. P. Singh, S. Singh, and B. K. Basu, Ferroelectrics **25**, 519 (1980).

[21]M. C. Pierre, J. P. Dufour, and M. Remoissenet, Solid State Commun. **9**, 1493 (1971).

[22]E. Litov and E. A. Uehling, Phys. Rev. B **1**, 3713 (1970).

[23]P. S. Peercy and G. A. Samara, Phys. Rev. B **8**, 2033 (1973).

[24]G. Hauret, L. Taurel, and J. P. Chapelle, Solid State Commun. **10**, 727 (1972); C. R. Acad. Sci. Paris Ser. B **273**, 627 (1971).

[25]C. W. Garland and D. B. Novotny, Phys. Rev. **177**, 971 (1969).